6p 19951081/4 324752

N95-14528

EXPERIMENTAL INVESTIGATION OF THE MARANGONI EFFECT ON THE STABILITY OF A DOUBLE-DIFFUSIVE LAYER

Josef Tanny and Chuan F. Chen
Department of Aerospace and Mechanical Engineering
The University of Arizona
Tucson, Arizona 85721

ABSTRACT

Stability experiments were carried out in a 4-cm-thick, salt-stratified fluid layer by heating from below and cooling from above. The bottom boundary was rigid while the top was either free or rigid. The initial solute Rayleigh number varied from 2.5×10^6 to 4.6×10^7. For the rigid-free case, at initial solute Rayleigh numbers $R_S > 5.4 \times 10^6$, thermal Marangoni instabilities were observed to onset along the free surface at a relatively low thermal Rayleigh number, R_T. The convection was very weak, and it had almost no effect on the concentration and temperature distributions. Double-diffusivè instabilities along the top free surface were observed to onset at a higher R_T, with much stronger convection causing changes in the concentration and temperature distributions near the top. At a yet higher R_T, double-diffusive convection was observed to onset along the bottom boundary. Fluid motion in the layer then evolved into fully developed thermal convection of a homogeneous fluid without any further increase in the imposed ΔT. For layers with $R_S < 5.4 \times 10^6$, Marangoni and double-diffusive instabilities onset simultaneously along the free surface first, while double-diffusive instabilities along the bottom wall onset at a higher R_T.

INTRODUCTION

The low-gravity environment in a space shuttle or a space station provides a unique opportunity to carry out experiments to study the interactions of surface tension and double-diffusive effects on the onset of instability and subsequent motion in a fluid layer. This problem not only has practical applications in materials processing in space, but also is of fundamental interest in understanding the behavior of fluids in response to the simultaneous inputs of stabilizing or destabilizing effects of surface and body forces.

When an alloy melt is solidified directionally by cooling from the bottom of the mold and the heavier element is preferentially crystallized out at the liquidus temperature, there is a region of vigorous finger convection above the mushy zone [see, for example, Chen and Chen (1991)]. Salt-finger convection is the result of a double-diffusive instability caused by the adverse density gradient generated by the slower diffusing component in the solution. It is easily demonstrated that using the property values of a lead-tin alloy as given by Coriell et al. (1980) and assuming a concentration difference of 0.5 wt% across a fluid layer depth of 1 cm, such convection will exist at 10^{-4} g_0, where g_0 is the gravitational acceleration at sea level. Such gravity levels were measured on board Skylab and shuttle missions at quiet times (Chassay and Schwaniger 1986). When a free surface is present, either due to shrinkage or an open mold, forces due to surface tension gradients become important and must be accounted for. The interactions between surface tension and double-diffusive effects may exacerbate or ameliorate the instability characteristics of the fluid layer. This will, in turn, affect the convection in the melt, which ultimately affects the quality of the casting.

The effect of surface tension on a fluid layer being heated from below was first studied by Nield (1964). Davis and Homsy (1980) generalized the problem to include the effect of a deformable free surface. McTaggart (1983) studied the stability of a layer with respect to surface tension effects when both temperature and concentration gradients are present in the layer. The layer is assumed to be in a zero-gravity environment. Recently, Chen and Su (1992) and Chen and Chen (1993) considered the combined Marangoni and double-diffusive instability problem including the effects of cross diffusion.

The effect of surface tension on the stability of a double-diffusive fluid was studied experimentally by Chen (1991). We have extended the investigation by conducting experiments over a range of initial solute Rayleigh numbers and by using an improved instrumentation and flow visualization technique. The results reported herein

not only provide a better understanding of the instability phenomenon but also will serve as a benchmark for the numerical simulation program based on the boundary element method currently under development.

EXPERIMENTAL APPARATUS AND PROCEDURES

The experiments were conducted in a rectangular test tank with inner dimensions of 24 × 12 × 5 cm high. The sidewalls of the tank were made of optical glass to facilitate Schlieren flow visualization. The top and bottom constant-temperature walls were made of stainless steel. In some of the experiments with the free surface, a brass top wall was used. In all cases, the removable top wall was provided with passages through which fluid from a constant-temperature bath could circulate. The tank was placed above an aluminum heat transfer plate, which was kept at a constant temperature by another constant-temperature bath. An RdF microfoil heat flux sensor with dimensions of 4 × 1.5 × 0.15 cm thick was placed between the stainless steel bottom and the plate. In order to minimize contact resistances, a thermal joint compound was applied to all contact surfaces. Thermocouples were embedded in the top and bottom walls near the inside surfaces. Their output was linearized and recorded using a data logger. The top and bottom walls were insulated with 5-cm-thick Styrofoam. The sidewalls were not insulated in order to allow for continuous flow visualization during the experiment. This did not seem to influence the results because the temperature differences attained were usually small (not more than 5°C above or below room temperature).

Vertical concentration and temperature profiles were measured by a dual probe consisting of a four-electrode micro-scale conductivity instrument (MSCI) and a thermocouple. The sensor of the MSCI and the thermocouple junction were located at the same vertical level, at a horizontal distance of 0.3 cm. The combined probe was traversed vertically through the stratified fluid at a constant speed of about 0.11 mm/sec, recording the conductivity and temperature each 10 seconds, which resulted in about 40 data points over the layer depth. Data were always recorded while the probe was traversed downward, with the two sensors ahead of the probe holder in order to minimize any disturbances at the measured region. The MSCI was calibrated before and after each experiment against six solutions of known concentration. For experiments with aqueous solutions of NaCl, the output voltage of the MSCI was translated into concentration using the local measured temperature and the relations given by Head (1983).

The convective motions were visualized using the Schlieren technique. The Schlieren system consisted of two spherical mirrors, 15.24 cm (6 inches) in diameter and 152.4 cm in focal length, a white light source, and a knife edge. The system was set up such that the circular parallel beam was passed horizontally through the mid-section of the tank, visualizing an approximately 16-cm section out of a total length of 24 cm. The output of the Schlieren system was imaged by a CCD camera and was displayed on a monitor and also recorded by time-lapse VCR for later reviewing.

In all experiments, the depth of the salt-stratified fluid layer was 4 cm. Stratification was obtained by filling the tank with eight layers of salt (NaCl) solution of equal thickness (0.5 cm) but with decreasing concentration. The filled tank was let stand for 2 hr. A one-dimensional time-dependent numerical calculation predicted that the eight-layer structure would become smooth by molecular diffusion within this time period; this was verified by the concentration profile measurement. During the 2-hr waiting period, the stratified fluid was brought to a uniform temperature by applying equal temperatures at the top and bottom walls.

The experiment was started by increasing the bottom wall temperature by 0.5°C and decreasing the top wall temperature by 0.5°C, thus imposing a temperature difference of 1°C across the layer. This temperature change was allowed to diffuse across the layer over a period of 50 min, the thermal diffusion time for a 2-cm-thick water layer. Then, an additional change of 1°C was imposed across the layer, and so on. In the experiments with a free surface, the top wall was placed 0.9 cm above the free surface and, because of the air gap, its temperature had to be reduced much more than 0.5°C for each adjustment. It was found by trial and error that a temperature reduction of 1.5°C was needed to reduce the free fluid surface temperature by 0.5°C. The vertical profiles of concentration and temperature were always measured before each temperature adjustment, when the system was in a quasi-steady state.

The temperature gradient was increased until double-diffusive instability plumes were observed at the bottom and top walls. In those experiments where instability started near one wall before the other, the temperature gradient was further increased until both the top and bottom regions became unstable. At this slightly supercritical condition, the system was allowed to stand for a few hours until a state of turbulent thermal convection across the layer was established.

RESULTS AND DISCUSSION

In this section, we first present the results of two experiments with the same initial stratification but with different boundary conditions in order to illustrate the effect of Marangoni instability on the stability characteristics of a double-diffusive layer. Experiment 18 was carried out with rigid-rigid (R-R) conditions, and experiment 30 was carried out with rigid-free (R-F) conditions. The initial salinity gradient was nominally the same, with the first 0.5 cm layer at 2.7 wt% and the top layer at 2.0 wt%. A series of six concentration profiles for both experiments are shown in Fig. 1 in order to illustrate the different phases of instability.

At t = 120 min after the filling of the test tank, the concentration profiles of isothermal fluid layers in the R-R (left) and R-F (right) cases are shown in Fig. 1a. The two profiles are essentially the same. The initial solute Rayleigh numbers, R_S, are 1.98×10^7 and 1.88×10^7, respectively. At t = 220 min, after two adjustments of ΔT, with the thermal Rayleigh number $R_T = 1.47 \times 10^6$ (Fig. 1b), Marangoni instability in the R-F case became observable in the Schlieren picture. We denote this critical thermal Rayleigh number by R_{T1}. The Marangoni convection cells appeared as short, vertical dark shadows, more or less equally spaced along the free surface. These are indicated in the sketch below the concentration profiles. The Marangoni convection was confined to the neighborhood of the free surface because of the stable density gradient in the fluid layer. The concentration of the fluid became uniform within a layer of 0.4 cm thickness below the free surface due to the convective mixing (Fig. 1b).

At t = 320 min and $R_T = 3.37 \times 10^6$, double-diffusive convection in the form of plumes (Shirtcliffe 1969) started near the free surface where the stabilizing salinity gradient was weakened by Marangoni convection. This critical Rayleigh number is denoted by R_{T2}. These plumes penetrated much deeper into the fluid, and the mixed layer extended down to approximately 0.8 cm (Fig. 1c). The upper mixed layer continued to deepen as ΔT was increased, and Marangoni convection cells disappeared as double-diffusive cells strengthened. At t = 370 min and $R_T = 4.03 \times 10^6$, it reached down to 1.3 cm (Fig. 1d). At t = 470, when R_T reached 4.97×10^6 (Fig. 1e), double-diffusive convection started at the bottom wall, which was clearly indicated by the concentration profile. This critical Rayleigh number is denoted by R_{T3}. At this time, the concentration profile in the R-R case was still evolving by diffusion. At t = 500-510 min (Fig. 1f), double-diffusive convection occurred both at the top and the bottom walls in the R-R case at $R_T = 6.96 \times 10^6$. In the terminology developed so far, for the R-R case, there is no R_{T1} and R_{T2} and R_{T3} approach each other. We denote this transition by $R_{T2,3} = 6.9 \times 10^6$. At that time, in the R-F case, the convection in both layers was well developed and the R_T actually decreased to 4.76×10^6 due to the slight drop in ΔT because of the four-fold increase in heat flux from the conductive state to the fully convective stage.

A total of thirteen experiments were conducted, seven of these were with rigid-free conditions and six with rigid-rigid conditions. Data from these experiments are shown in Fig. 2, in which the critical thermal Rayleigh number is shown as a function of the solute Rayleigh number. The initial solute Rayleigh number varied from 2.5×10^6 to 4.6×10^7. For the R-F cases, when $R_S > 5.4 \times 10^6$, the sequence of events is similar to what we described above: there are three distinct thermal Rayleigh numbers, R_{T1} (denoted by crosses), R_{T2} (denoted by filled squares), and R_{T3} (denoted by filled circles). But, for the two experiments with initial $R_S < 5.4 \times 10^6$, onset of Marangoni and double-diffusive instability at the top occurred simultaneously, thus $R_{T1} = R_{T2}$. For the R-R case, in general, double-diffusive instability at the bottom (denoted by open circles) and at the top (denoted by open squares) occurred at the same thermal Rayleigh number, $R_{T2} = R_{T3} = R_{T2,3}$. In this case, there is no R_{T1}. It is seen that due to the thermal Marangoni effect, the fluid layer with the R-F condition is less stable than that with the R-R condition.

Straight lines were fitted through the data points by the least squares method. For the R-F cases with $R_S > 5.4 \times 10^6$, R_{T1} is nearly a horizontal line:

$$R_{T1} = 5.012 \times 10^5 R_S^{0.07} \qquad 5.4 \times 10^6 < R_S < 4.6 \times 10^7$$

while R_{T2} and $R_{T3} \propto R_S^{0.771}$ and $R_S^{0.7}$, respectively:

$$\left.\begin{aligned} R_{T2} &= 10.695 \times R_S^{0.771} \\ R_{T3} &= 54.828 \times R_S^{0.7} \end{aligned}\right\} \qquad 2.5 \times 10^6 < R_S < 4.6 \times 10^7$$

For the R-R case, double-diffusive convection onsets simultaneously along the bottom and top walls, with one exception. A straight line correlation yields the following:

$$R_{T2,3} = 116.95 R_S^{0.664}$$

The full line denotes the theoretical onset condition for double-diffusive convection in a layer with linear gradients and stress-free boundaries, $R_{T2,3} \propto R_S$ (Turner 1973).

CONCLUSIONS

1. For a double-diffusive layer with a free surface, at high initial solute Rayleigh numbers ($R_S > 5.4 \times 10^6$), the first instability to occur is the Marangoni instability at the free surface. At successively higher thermal Rayleigh numbers, double-diffusive instability first appears at the free surface, then at the bottom rigid surface.

2. At lower initial solute Rayleigh numbers ($R_S < 5.4 \times 10^6$), Marangoni and double-diffusive instabilities occur simultaneously at the free surface. Double-diffusive instability appears at the bottom rigid boundary at a higher thermal Rayleigh number.

3. Although the Marangoni convection at the free surface is not strong enough to affect the concentration and temperature distributions, it contributes substantially to the reduction in the critical thermal Rayleigh number for the onset of double-diffusive convection, both at the top and the bottom of the layer.

ACKNOWLEDGEMENTS

The financial support provided by NASA MSAD through grant NAG3-1386 is gratefully acknowledged.

REFERENCES

Chassay, R. P. and Schwaniger, A. J., 1986, NASA TM-86585.
Chen, C. F., 1991, Microgravity Sci. and Tech., 4, 108-109.
Chen, C. F. and Chen, C. C., 1993, Phys. Fluids, 6, 1482-1490.
Chen, C. F. and Chen, F., 1991, J. Fluid Mech., 227, 567-586.
Chen, C. F. and Su, T. F., 1992, Phys. Fluids A, 11, 2360-2367.
Coriell, S. R., Cordes, M. R., Boettinger, W. J., and Sekerka, R. F., 1980, J. Cryst. Growth, 49, 13-28.
Davis, S. H. and Homsy, G. M., 1980, J. Fluid Mech., 98, 527-553.
Head, M. J., 1983, Ph.D. Thesis, University of California, San Diego.
McTaggart, C. A., 1983, J. Fluid Mech., 134, 301-310.
Nield, D. A., 1964, J. Fluid Mech., 19, 341-352.
Shirtcliffe, T. G. L., 1969, J. Fluid Mech., 35, 677-688.
Turner, J. S., 1973, Buoyancy Effects in Fluids, Cambridge University Press, p. 255.

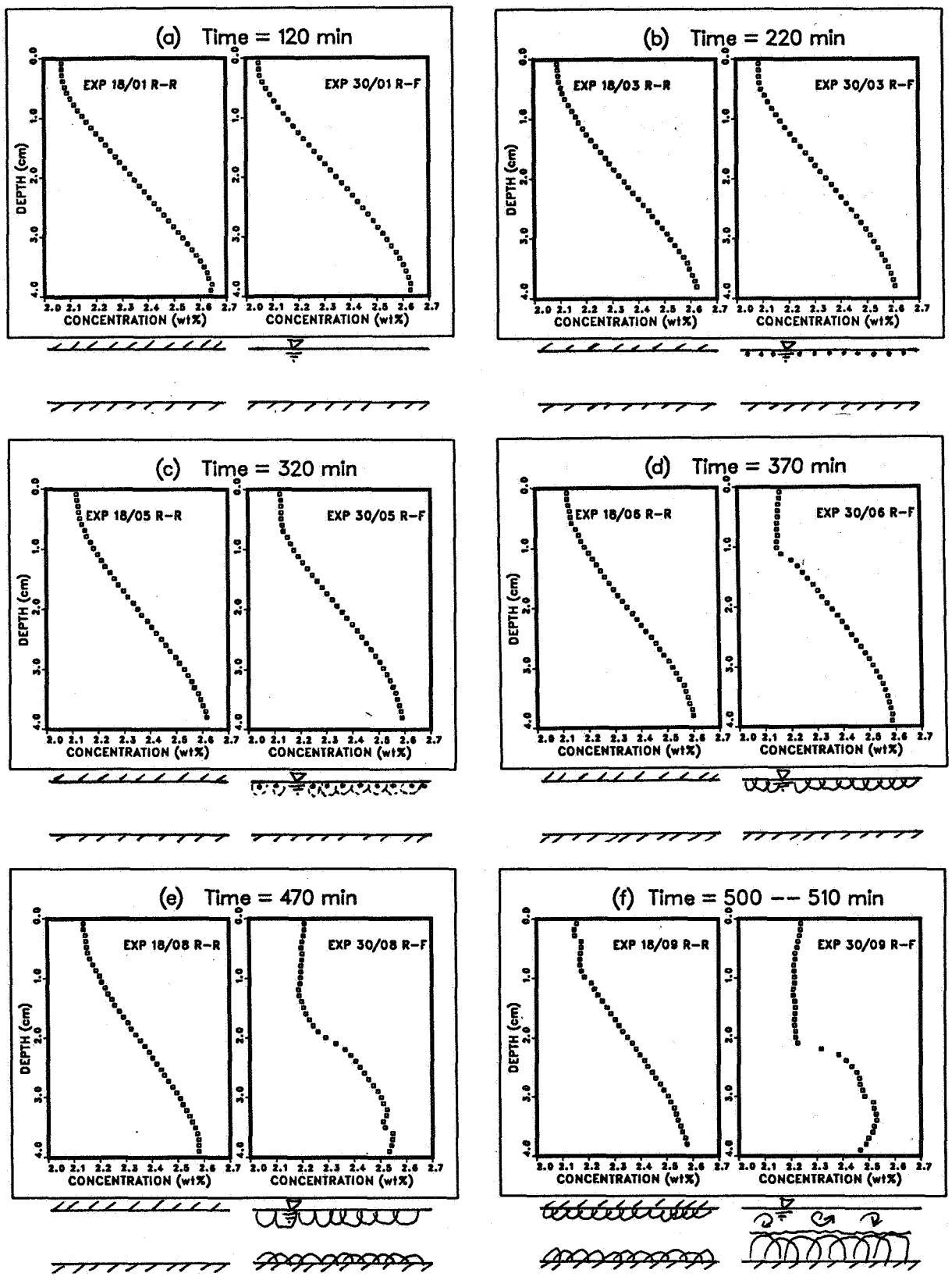

Fig. 1. Evolution of concentration profile for the R-R case (left) and the R-F case (right) as R_T is increased. Sketch below each graph illustrates the flow pattern observed.

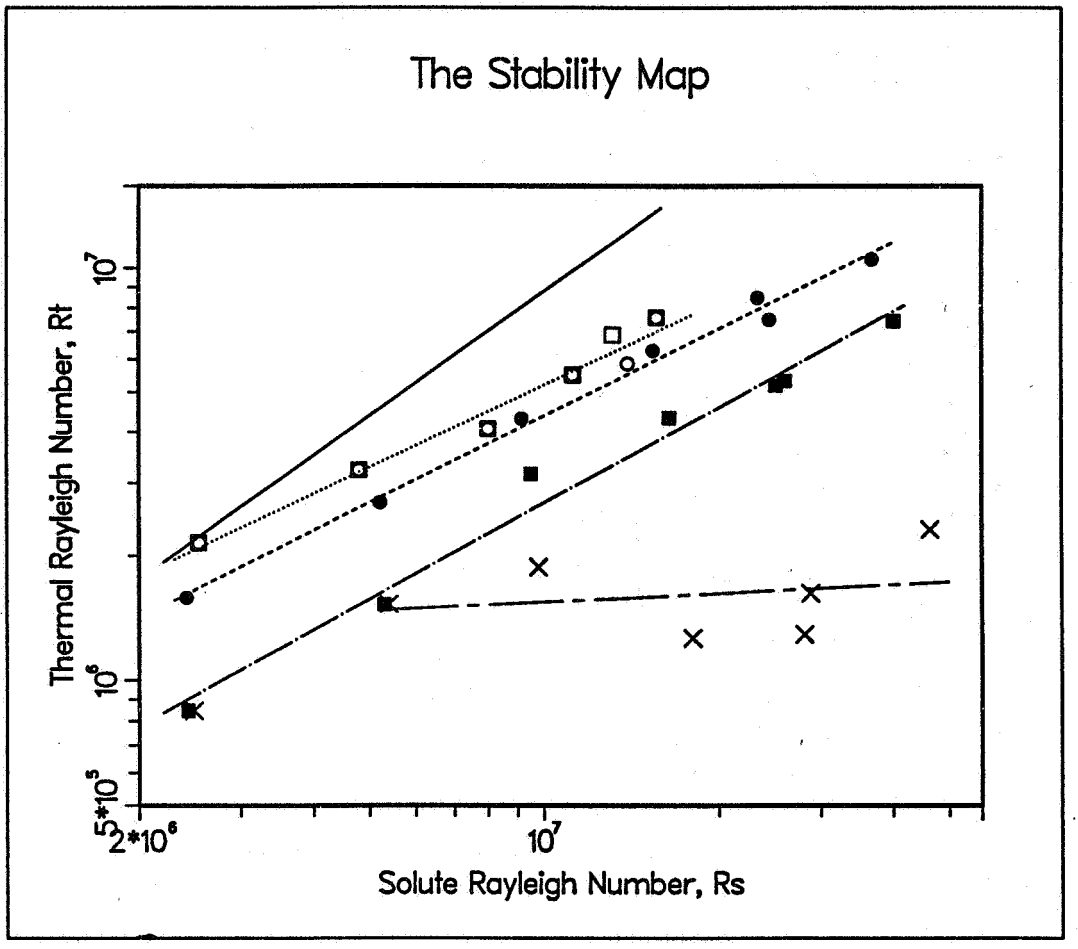

Fig. 2. The stability map. × Marangoni instability; ■, ● double-diffusive instability at the top and the bottom, respectively, for the R-F case; □, O double-diffusive instability at the top and the bottom, respectively, for the R-R case; —— theoretical result.